JOURNAL OF SOLID STATE CHEMISTRY **135,** 302–306 (1998)
ARTICLE NO. SC977641

A Mixed-Valent Vanadium Monophosphate with a Chain-Like Structure: $Ba_3V_2O_3(PO_4)_3$

M. M. Borel, A. Leclaire, J. Chardon, C. Michel, J. Provost, and B. Raveau

Laboratoire CRISMAT, UMR 6508 associée au CNRS, ISMRA et Université de Caen, 6, Boulevard du Maréchal Juin, 14050 Caen Cedex, France

Received June 30, 1997; in revised form October 1, 1997; accepted October 6, 1997

A new mixed-valence vanadium monophosphate with a chain-like structure has been synthesized. It crystallizes in the $P2_12_12_1$ space group with $a = 5.137(1)$, $b = 12.418(1)$, and $c = 20.724(3)$ Å. The structure consists of $[V_2P_3O_{15}]_\infty$ ribbons running along a, whose cohesion is ensured by Ba^{2+} cations. Each ribbon is built from two sorts of chains: $[VPO_7]_\infty$ chains, which consist of corner-sharing VO_5 trigonal bipyramids and PO_4 tetrahedra, and $[VP_2O_{10}]_\infty$ chains built of VO_6 octahedra and PO_4 tetrahedra. The vanadium-centered polyhedra are linked together by corner-sharing, so that V_2O_{10} units are formed. Charge ordering is observed on the vanadium species, with V(IV) in the octahedron and V(V) in the bipyramid. © 1998 Academic Press

INTRODUCTION

Vanadium phosphates are of great interest due to the possible mixed valence of vanadium, which is often the origin of its peculiar electron transport, magnetic, or catalytic properties. For this reason, numerous mixed-valent vanadium phosphates have been synthesized in the past 15 years. Most of them are characterized by a tridimensional framework forming either cages or tunnels in which univalent or divalent cations are located. Several vanadophosphates exhibit a bidimensional structure, although they are much less numerous. In contrast, very few vanadium phosphates with a chain-like structure have been synthesized to date. In this respect, the barium-based vanadophosphates may be of interest because the monophosphate $Ba_2VO(PO_4)_2 \cdot H_2O$ exhibits an unidimensional structure (1). This compound is the only one in the system Ba–V–P–O that presents such a chain-like structure. In particular, all the phosphates of this system prepared to date by direct synthesis exhibit a tridimensional structure in anhydra phases. This is the case of α- and β-$BaV_2P_2O_7$ (2–3), $Ba_3V_4(PO_4)_6$ (4) and $BaVO_2PO_4$ (6). Thus, it seems that the unidimensional structure of $Ba_2VO(PO_4)_2 \cdot H_2O$ is stabilized by the presence of H_2O, which is incorporated during hydrothermal synthesis.

The analysis of such chain-like structures suggests that the interchain species (barium) is rather numerous with respect to the elements forming the chains (V, P) to avoid the formation of "V–P–O" layers, or 3-D frameworks. For this reason we have reinvestigated, via solid state chemistry techniques, the Ba–V–O–P system for higher barium contents, i.e. $Ba/V > 1$ and $Ba/P \cong 1$. In the present paper we report on the mixed-valent vanadium monophosphate $Ba_3V_2O_3(PO_4)_3$, which exhibits an original structure characterized by charge ordering in the vanadium sites.

EXPERIMENTAL SECTION

Crystal Growth

Single crystals of the title compound were grown from a mixture of nominal composition $Ba_3V_2P_4O_{18} \cdot BaCO_3$, V_2O_5, and $H(NH_4)_2PO_4$ were mixed in appropriate ratios and heated in a platinum crucible in air to 873 K for 12 h to eliminate H_2O, CO_2, and NH_3. The mixture was ground again and heated at 973 K in air for 12 h, and finally quenched to room temperature.

In the resulting mixture two sorts of crystals were extracted: blue plate-like crystals that were always twinned, and yellow needle-like crystals whose cationic composition was determined by microprobe analysis. The latter were studied by X-ray diffraction.

Chemical Synthesis

The quantitative synthesis of polycrystalline samples of the phosphate $Ba_3V_2O_3(PO_4)_3$ was performed in two steps. First mixture of $Ba(NO_3)_2$, NH_4VO_3, and $H(NH_4)_2PO_4$ in appropriate ratios according to the composition $Ba_3V_{1.8}P_3O_{15}$ was heated at 673 K in a platinum crucible to decompose the barium nitrate, the ammonium vanadate, and the ammonium phosphate. In a second step, the resulting mixture was then added to the required amount of metallic vanadium (0.2 mol), sealed in an evacuated silica ampoule, and heated for 12 h at 1023 K, then quenched to room temperature.

0022-4596/98 $25.00

Energy Dispersive Spectroscopy (EDS)

The cationic composition was performed by EDS using a Tracor microprobe mounted on a scanning microscope. The cationic composition $Ba_3V_2P_3$ was found for all the yellow crystals.

X-ray Diffraction

A yellow needle with dimensions $0.103 \times 0.045 \times 0.013$ mm was selected for the structure determination. The cell parameters were determined by diffractometric techniques at 294 K with a least square refinement based on 25 reflections with $18^\circ < \theta < 22^\circ$. The data were collected on a CAD4 ENRAF NONIUS diffractometer with the parameters reported in Table 1. The systematic extinctions $h = 2n + 1$ for $h00$, $k = 2n + 1$ for $0k0$, and $l = 2n + 1$ for $00l$ are consistent with the space group $P2_12_12_1$. The reflections were corrected for Lorentz and polarization effects and for absorption by the gaussian method. The structure was solved with the heavy atom method. The final refinement included atomic coordinates, and their anisotropic thermal parameters for Ba, V, and P, and their isotropic thermal parameters for oxygen led to $R = 0.036$ and $R_W = 0.032$. Results are listed in Table 2.

TABLE 1
Summary of Crystal Data, Intensity Measurements, and Structure Refinement Parameters for $Ba_3V_2O_3(PO_4)_3$

1. Crystal Data	
Space group	$P2_12_12_1$
Cell dimensions	$a = 5.137(1)$ Å
	$b = 12.418(1)$ Å
	$c = 20.724(3)$ Å
Volume (Å)^3	1322.0(3) Å^3
Z	4
d_{calc} (g·cm^{-3})	4.25
2. Intensity Measurements	
λ(Mo$K\alpha$)	0.71073
Scan mode	ω–2/3θ
Scan width (°)	$1.1 + 0.35 \tan\theta$
Slit aperture (mm)	$1.3 + \tan\theta$
Max θ (°)	45
Standard reflections	3 measured every 3600 s
Measured reflections	11382
Reflections with $I > 3\sigma$	2930
μ (mm^{-1})	10.61
Transmission	0.585–0.789
3. Structure Solution and Refinement	
Parameters refined	134
Agreement factors	$R(F) = 0.036$ $R_w(F) = 0.032$
Weighting scheme	$w = 1/\sigma^2$
Δ/σ max	< 0.0001
$\Delta\rho$(e Å^{-3})	2

TABLE 2
Atomic Positional, Isotropic, and Anisotropic Displacement Parameters

	Positional and Isotropic Displacement Parameters				
	x/a	y/b	z/c		U
Ba(1)	0.3046(1)	0.37282(5)	0.93554(3)	*	0.0102(2)
Ba(2)	0.2925(1)	0.21838(4)	0.25645(3)	*	0.0093(2)
Ba(3)	0.2245(1)	0.36096(5)	0.57964(3)	*	0.0108(2)
V(1)	0.2158(4)	0.0570(1)	0.65135(8)	*	0.0074(4)
V(2)	0.3270(4)	0.1080(1)	0.82043(8)	*	0.0074(5)
P(1)	0.2195(6)	0.3250(2)	0.4113(1)	*	0.0076(7)
P(2)	0.2007(6)	0.5362(2)	0.2622(1)	*	0.0086(7)
P(3)	0.3115(6)	0.3175(2)	0.0939(1)	*	0.0077(7)
O(1)	0.210(2)	−0.0046(6)	0.5839(3)		0.016(1)
O(2)	−0.032(1)	0.1782(6)	0.6324(4)		0.006(1)
O(3)	0.490(1)	0.1687(6)	0.6372(4)		0.010(2)
O(4)	0.465(1)	−0.0488(7)	0.6926(4)		0.014(2)
O(5)	−0.055(1)	−0.0345(7)	0.6948(4)		0.013(2)
O(6)	0.212(1)	0.1346(5)	0.7482(3)		0.011(1)
O(7)	0.250(2)	−0.0139(6)	0.8407(4)		0.018(2)
O(8)	0.570(1)	0.2097(6)	0.8616(4)		0.009(2)
O(9)	0.061(1)	0.1964(6)	0.8625(4)		0.009(2)
O(10)	0.670(2)	0.0692(6)	0.7774(3)		0.014(2)
O(11)	0.292(2)	0.4304(6)	0.0666(4)		0.016(2)
O(12)	0.327(2)	0.2311(6)	0.0430(3)		0.012(2)
O(13)	0.209(2)	0.2175(6)	0.4459(3)		0.014(1)
O(14)	0.221(2)	0.4198(5)	0.4561(3)		0.010(1)
O(15)	0.213(2)	0.6340(5)	0.2176(3)		0.011(1)

	Anisotropic Displacement Parameters					
	$U11$	$U22$	$U33$	$U12$	$U13$	$U23$
Ba(1)	0.0123(3)	0.0095(3)	0.0089(3)	−0.0006(3)	0.0006(3)	−0.0005(2)
Ba(2)	0.0092(3)	0.0093(2)	0.0093(3)	−0.0007(3)	−0.0007(3)	−0.0007(2)
Ba(3)	0.0120(3)	0.0099(3)	0.0107(3)	0.0003(3)	0.0007(3)	0.0024(2)
V(1)	0.0083(8)	0.0077(7)	0.0062(7)	−0.0002(7)	0.0012(7)	0.0004(6)
V(2)	0.0063(9)	0.0081(7)	0.0077(7)	−0.0009(7)	0.0000(7)	−0.0007(6)
P(1)	0.009(1)	0.007(1)	0.007(1)	0.000(1)	0.001(1)	0.0004(9)
P(2)	0.007(1)	0.009(1)	0.010(1)	−0.000(1)	−0.000(1)	−0.001(1)
P(3)	0.011(1)	0.006(1)	0.006(1)	0.003(1)	−0.001(1)	−0.0026(9)

Thermogravimetric Analysis in Oxygen

The microthermogravimetric analysis was performed in an oxygen flow using a Setaram microbalance. The sample was heated to 900°C at a speed of 150°C h^{-1}. The weight gain of 0.95% is in perfect agreement with the oxidation of one V (IV) per formula $Ba_3V_2O_3(PO_4)_3$ (theoretical value, 0.94%).

Magnetic Measurements

The magnetic susceptibility of powdered samples was investigated by SQUID magnetometry in the temperature range 4–5 and 350 K. The zero field-cooled magnetic moment of the sample was measured in a field of 0.3 T. The magnetic moment of the sample holder was measured in the same temperature range under the same magnetic field. The sample holder moment was then subtracted from the measured total moment.

Finely ground powdered samples were used for recording the EPR spectra. Variable-temperature X band spectra at

300 and 77 K were recorded in a Brüker (ER 200) spectrometer fitted with double cavity TE_{110}. For these temperatures, 100 kHz magnetic field modulation was used. The measured g values were calibrated with respect to the Brüker strong pitch ($g = 2.0028$).

RESULTS AND DISCUSSION

Structure

The projection of the structure along **a** (Fig. 1) shows its unidimensional character. It consists of $[V_2P_3O_{15}]_\infty$ ribbons running along **a** whose cohesion is ensured through Ba^{2+} cations. The $[V_2P_3O_{15}]_\infty$ ribbons are displayed in layers parallel to (001). As shown from the projection of the ribbons along **b** (Fig. 2), the $[V_2P_3O_{15}]_\infty$ ribbons that form the structure are identical, but exhibit two different orientations respective to the 2_1 axis.

Each $[V_2P_3O_{15}]_\infty$ ribbon is built of two kinds of chains. $[VP_2O_{10}]_\infty$ and $[VPO_7]_\infty$ respectively. In the first type of chain, one VO_6 octahedron (V(1)) alternates with two PO_4 tetrahedra (P(1) and P(2)) along **a** in a way similar to that observed in $Ba_2VO(PO_4)_2H_2O$ (1) and $BaMo(PO_4)_2$ (7). In the $[VPO_7]_\infty$ chain, one VO_5 trigonal bipyramid (V(2)) alternates with one PO_4 tetrahedron (P(3)) along **a**. Thus, the $[V_2P_3O_{15}]_\infty$ ribbon results from assembling one $[VPO_7]_\infty$ chain with one $[VP_2O_{10}]_\infty$ chain in such a way that each VO_5 bipyramid of the first chain shares one apex with one VO_6 octahedron, and one apex with one PO_4 tetrahedron of the second chain. In the same way, each VO_6 octahedron of the second chain shares one apex with one VO_5 bipyramid and one apex with one PO_4 tetrahedron of the first chain. Consequently each trigonal bipyramid V(2), each octahedron V(1), and each tetrahedron P(2) exhibits one free apex, while each P(1) and P(3) tetrahedron exhibits two free apexes. An interesting feature of this structure concerns the existence of isolated V_2O_{10} units built of one VO_6 octahedron and one VO_5 bipyramid sharing one apex. Such a unit has previously been observed in the phosphate $AMo_3O_4(PO_4)_3$ (A = Li, Ag, Na) (8–10).

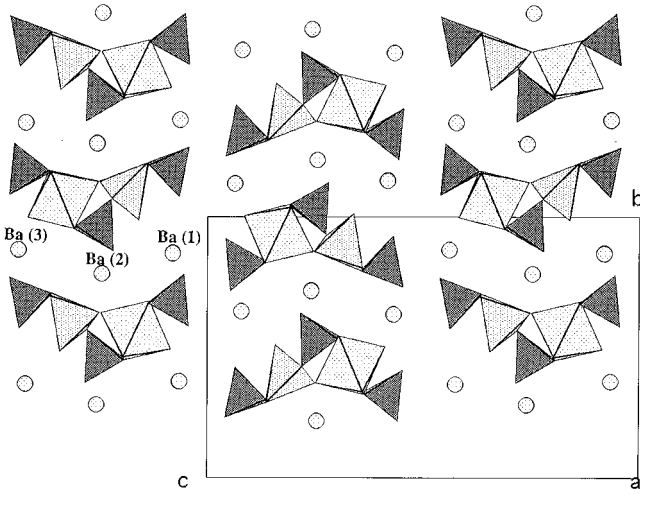

FIG. 1. Projection of the structure of $Ba_3V_2O_3(PO_4)_3$ along **a**.

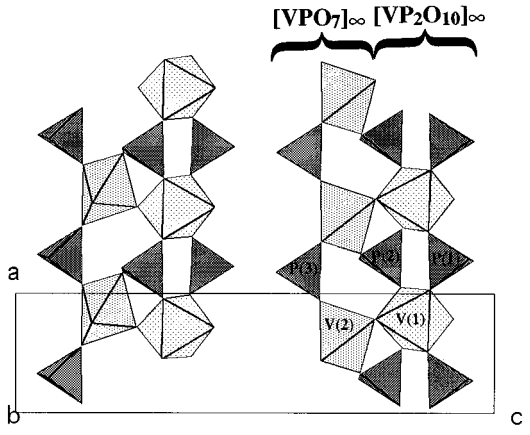

FIG. 2. Projection of the $[V_2P_2O_{15}]_\infty$ ribbons along **b**.

Thus, the P(1) and P(3) tetrahedra are linked to two octahedra and two bipyramids respectively. Consequently, their P–O distances (Table 3) show that they are slightly distorted, with two shorter P–O distances (1.498 to 1.515 Å) corresponding to the two free apexes and two longer ones (1.554 to 1.582 Å) corresponding to the P–O–V bonds. Each P(2) tetrahedron is linked to two V(1) octahedra and one V(2) bipyramid, so its geometry is almost regular, with one shorter P–O distance (1.527 Å) corresponding to its free apex and three longer P–O distances (1.537 to 1.553 Å) corresponding to P–O–V bonds.

The geometry of the VO_6 octahedron is characteristic of the vanadyl species, suggesting that the V(1) site is occupied by tetravalent vanadium. One indeed observes an abnormally short V–O distance (1.593 Å) corresponding to the free oxygen apex compared to a very long one (2.227 Å) corresponding to a V–O–V bond. The four intermediate equatorial V–O distances (1.997 to 2.023Å) correspond to V–O–P bonds, as classically observed in many phosphates of transition elements.

The VO_5 bipyramid exhibits two short distances, corresponding to the free apex (1.619 Å) and the V–O–V bond with the VO_6 octahedron (1.64 Å). The three other distances, which correspond to V–O–P bonds, are normal (1.95 to 2.032 Å).

Three sorts of barium cations ensure the cohesion of the structure. Ba(1) and Ba(2) exhibit an 11-fold coordination with Ba(1)–O distances ranging from 2.614 to 3.204 Å and Ba(2)–O distances ranging from 2.786 to 3.090 Å. A ninefold coordination is observed for Ba(3), with Ba(3)–O distances ranging from 2.607 to 3.329 Å. The geometry of the BaO_{11} and BaO_9 polyhedra is not regular.

TABLE 3
Distances (Å) and Angles (°) in the Polyhedra for $Ba_3V_2O_3(PO_4)_3$

V(1)	O(1)	O(2)	O(3)	O(4)	O(5)	O(6)
O(1)	**1.593(7)**	2.78(1)	2.81(1)	2.66(1)	2.70(1)	3.82(1)
O(2)	100.2(4)	**2.009(7)**	2.68(1)	4.00(1)	2.94(1)	2.76(1)
O(3)	102.6(4)	84.1(3)	**1.997(8)**	2.94(1)	3.95(1)	2.74(1)
O(4)	94.1(4)	165.7(4)	93.9(4)	**2.023(8)**	2.68(1)	2.86(1)
O(5)	96.3(4)	94.1(3)	161.1(4)	83.3(4)	**2.011(8)**	2.74(1)
O(6)	176.6(4)	81.2(3)	80.7(3)	84.6(3)	80.5(3)	**2.227(7)**

V(2)	O(6)	O(7)	O(8)	O(9)	O(10)
O(6)	**1.642(7)**	2.67(1)	3.13(1)	2.61(1)	2.56(1)
O(7)	109.7(4)	**1.619(8)**	3.26(1)	2.82(1)	2.73(1)
O(8)	119.6(4)	129.9(4)	**1.971(8)**	2.62(1)	2.52(1)
O(9)	92.4(4)	103.8(4)	83.6(3)	**1.957(8)**	3.92(1)
O(10)	87.7(4)	96.0(4)	78.0(3)	158.9(3)	**2.032(8)**

P(1)	$O(2^{i})$	$O(3^{ii})$	O(13)	O(14)
$O(2^{i})$	**1.567(9)**	2.46(1)	2.47(1)	2.54(1)
$O(3^{ii})$	104.2(4)	**1.554(8)**	2.50(1)	2.52(1)
O(13)	106.2(4)	108.9(4)	**1.516(8)**	2.52(1)
O(14)	111.9(4)	111.5(4)	113.5(4)	**1.498(7)**

P(2)	$O(4^{ii})$	$O(5^{i})$	$O(10^{ii})$	O(15)
$O(4^{ii})$	**1.540(9)**	2.47(1)	2.52(1)	2.49(1)
$O(5^{i})$	106.8(4)	**1.537(9)**	2.56(1)	2.50(1)
$O(10^{ii})$	109.1(4)	112.2(4)	**1.553(9)**	2.54(1)
O(15)	108.6(4)	109.2(4)	110.8(4)	**1.527(7)**

P(3)	$O(8^{ii})$	$O(9^{i})$	O(11)	O(12)
$O(8^{ii})$	**1.582(8)**	2.53(1)	2.56(1)	2.49(1)
$O(9^{i})$	106.3(4)	**1.580(8)**	2.56(1)	2.47(1)
O(11)	111.2(4)	111.7(4)	**1.515(8)**	2.53(1)
O(12)	107.3(4)	106.3(4)	113.6(4)	**1.506(8)**

Ba(1)–$O(14^{iii})$:	2.614(7)	Ba(2)–$O(2^{i})$:	2.786(7)	Ba(3)–$O(11^{iii})$:	2.607(7)
Ba(1)–$O(11^{iv})$:	2.808(7)	Ba(2)–$O(10^{ii})$:	2.801(7)	Ba(3)–O(14):	2.663(7)
Ba(1)–$O(12^{ii})$:	2.809(7)	Ba(2)–$O(15^{vii})$:	2.802(7)	Ba(3)–$O(13^{i})$:	2.726(7)
Ba(1)–$O(12^{iv})$:	2.840(7)	Ba(2)–$O(4^{viii})$:	2.818(7)	Ba(3)–O(2):	2.843(7)
Ba(1)–O(8):	2.883(7)	Ba(2)–$O(6^{i})$:	2.826(7)	Ba(3)–$O(13^{ii})$:	2.871(7)
Ba(1)–O(9):	2.941(7)	Ba(2)–$O(8^{ii})$:	2.845(7)	Ba(3)–$O(15^{iii})$:	2.878(7)
Ba(1)–$O(1^{v})$:	2.950(7)	Ba(2)–$O(15^{ix})$:	2.850(7)	Ba(3)–O(3):	2.996(7)
Ba(1)–$O(12^{i})$:	3.010(7)	Ba(2)–$O(5^{vii})$:	2.944(7)	Ba(3)–O(13):	3.295(7)
Ba(1)–$O(4^{v})$:	3.066(7)	Ba(2)–$O(9^{i})$:	3.018(7)	Ba(3)–$O(7^{vi})$:	3.329(7)
Ba(1)–$O(1^{vi})$:	3.077(7)	Ba(2)–$O(3^{ii})$:	3.040(7)		
Ba(1)–$O(5^{vi})$:	3.204(7)	Ba(2)–$O(7^{vii})$:	3.090(7)		

Symmetry codes

i:	$1/2 + x$; $1/2 - y$; $1 - z$
ii:	$-3/2 + x$; $1/2 - y$; $1 - z$
iii:	$1/2 - x$; $1 - y$; $1/2 + z$
iv:	x; y; $1 + z$
v:	$1 - x$; $1/2 + y$; $3/2 - z$
vi:	$-x$; $1/2 + y$; $3/2 - z$
vii:	$1 - x$; $-1/2 + y$; $1/2 - z$
viii:	$1/2 - x$; $-y$; $1/2 + z$
ix:	$-x$; $-1/2 + y$; $1/2 - z$

Evidence for Charge Ordering

The microthermogravimetric measurement indicates an oxidation state of 4.5 for vanadium, in agreement with the structure determination. The existence of isolated V_2O_{10} units linked only through PO_4 tetrahedra suggests that electronic delocalization along the chains is possible. Nevertheless, the issue of electronic transfer between the VO_6 octahedron and the VO_5 pyramid of the V_2O_{10} has to be answered.

The calculation of valences using the Brese and O'Keeffe (11) theory leads to the valence states 4.15 and 4.8 for V(1) and V(2) respectively. Clearly, charge ordering is observed, with V(IV) in the octahedron and V(V) in the trigonal bipyramid, despite the fact that the two polyhedra, V(1) and V(2), share one apex. Such a strong electronic localization is in agreement with the nature of the V(1)–O–V(2) bond, which is characterized by an abnormally long V(1)–O distance (2.227 Å) in the VO_6 octahedron and a short V(2)–O distance (1.642 Å) in the VO_5 bipyramid, so these two polyhedra can be considered weakly connected.

The molar susceptibility curve versus temperature (Fig. 3) confirms the electronic localization. Paramagnetic behavior with fitting parameters in the high-temperature range of the $\chi(T)$ curves is observed, leading to a magnetic moment of 1.62 μ_B. This result is in agreement with the existence of one V(IV) species per molar unit ($\mu_{th} = 1.73$). An antiferromagnetic transition occurs at $T = 25$ K (Fig. 3).

The room temperature EPR spectrum is shown in Fig. 4. It exhibits a very strong signal characterized by one approximately symmetrical, unresolved lineshape. The absence of hyperfine structure is due to the high concentration of paramagnetic ions. The calculated g_{iso} value, $g_{iso} = 1.965$, is quite comparable to that measured for compounds containing vanadyl ions (12) and confirms the electron localization in the VO_6 octahedron. At liquid nitrogen temperature, the spectrum is similar to the one recorded at room temperature, and no change in the g value is observed.

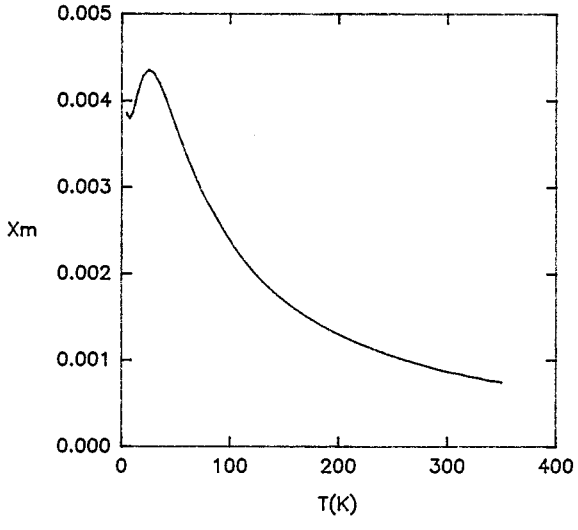

FIG. 3. Molar magnetic susceptibility χ_m vs temperature.

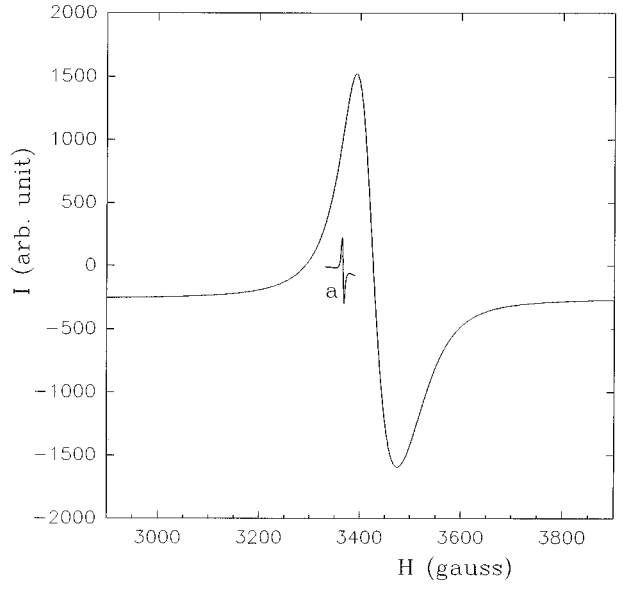

FIG. 4. Room temperature EPR spectrum. The signal of Ref. (4). ($g_0 = 2.0028$, $H_0 = 3366$G) is given as a guide.

REFERENCES

1. W. T. Harrison, S. C. Lim, J. T. Vaughey, A. J. Jacobson, D. P. Goshorn, and J. W. Johnson, *J. Solid State Chem.* **113,** 444 (1994).
2. L. Benhamada, A. Grandin, M. M. Borel, A. Leclaire, and B. Raveau, *Acta Crystallogr. Sect. C* **47,** 2437 (1991).
3. S. J. Hwu, R. I. Carroll, and D. L. Serra, *J. Solid State Chem.* **110,** 290 (1994).
4. K. Kasthuri Rangan, and J. Gopalakrishnan, *J. Solid State Chem.* **109,** 116 (1994).
5. A. Grandin, J. Chardon, M. M. Borel, A. Leclaire, and B. Raveau, *J. Solid State Chem.* **99,** 297 (1992).
6. H. Y. Kang and S. L. Wang, *Acta Crystallogr. Sect. C* **48,** 975 (1992).
7. A. Leclaire, M. M. Borel, J. Chardon, and B. Raveau, *J. Solid State Chem.* **116,** 364 (1995).
8. T. Hoareau, M. M. Borel, A. Leclaire, J. Provost, and B. Raveau, *Mat. Res. Bull.* **30,** 523 (1995).
9. G. Costentin, M. M. Borel, A. Grandin, A. Leclaire, and B. Raveau, *J. Solid State Chem.* **95,** 168 (1991).
10. A. Guesdon, M. M. Borel, A. Grandin, A. Leclaire, and B. Raveau, *C.R. Acad. Sciences* **316,** 477 (1993).
11. N. E. Brese and M. O'Keeffe, *Acta Crystallogr. Sect. B* **47,** 192 (1991).
12. C. G. Ballhausen and H. B. Gray, *Inorg. Chem.* **1,** 111 (1962).